Journal of Organometallic Chemistry 694 (2009) 1122–1133

Contents lists available at ScienceDirect

Journal of Organometallic Chemistry

journal homepage: www.elsevier.com/locate/jorganchem

Structure, electrochemistry, spectroscopy, and magnetic resonance, including high-field EPR, of $\{(\mu\text{-abpy})[Re(CO)_3X]_2\}^{o/\bullet-}$, where abpy = 2,2′-azobispyridine and X = F, Cl, Br, I

Stéphanie Frantz [a], Monika Sieger [a], Ingo Hartenbach [a], Falk Lissner [a], Thomas Schleid [a], Jan Fiedler [b], Carole Duboc [c], Wolfgang Kaim [a,*]

[a] Institut für Anorganische Chemie, Universität Stuttgart, Pfaffenwaldring 55, D-70550 Stuttgart, Germany
[b] J. Heyrovský Institute of Physical Chemistry, v.v.i., Academy of Sciences of the Czech Republic, Dolejškova 3, CZ-18223 Prague, Czech Republic
[c] Grenoble High Magnetic Field Laboratory, Laboratoire des Champs Magnétiques Intenses CNRS, 25, Avenue des Martyrs, BP 166, F-38042 Grenoble Cedex 9, France

ARTICLE INFO

Article history:
Received 28 July 2008
Received in revised form 3 September 2008
Accepted 22 September 2008
Available online 27 September 2008

Keywords:
Azo ligand
Crystal structures
EPR
Rhenium dinuclear compounds
Spectroelectrochemistry

ABSTRACT

Attempts to prepare and study the title complexes yielded the structurally characterized neutral compounds *anti*-$\{(\mu\text{-abpy})[Re(CO)_3X]_2\}$, X = Br ($I4_1/a$), I ($C2/c$), and two crystalline forms of *anti*-$\{(\mu\text{-abpy})[Re(CO)_3Cl]_2\}$. One of these forms ($P2_1/c$) has been reported before, the other ($I4_1/a$), obtained through crystallization in the presence of Zn, is isostructural to the form found for *anti*-$\{(\mu\text{-abpy})[Re(CO)_3Br]_2\}$. Syntheses of $\{(\mu\text{-abpy})[Re(CO)_3Cl]_2\}$ at high or low temperatures yielded different compositions, the high temperature procedure led to partial formation of *syn*/*anti* mixtures and one-electron reduced species. The same was observed to a greater extent in the preparation of labile *syn*/*anti*-$\{(\mu\text{-abpy})[Re(CO)_3F]_2\}^{o/\bullet-}$. The identity of isolated species was investigated using ^1H NMR spectroscopy, variable frequency EPR spectroscopy, cyclic voltammetry, UV/Vis- and IR-spectroelectrochemistry. The effects of halide variation on structure, reduction potentials, isomerism and electronic situation are being discussed.

1. Introduction

Complexes $(N\text{–}N)Re(CO)_3X$, X = halogen, with unsaturated α-diimine chelate ligands (N–N), including 2,2′-bipyridine or 1,10-phenanthroline, have raised attention because of their photoemission [1], their energy and charge transfer properties [2], and their photo- and electrocatalytic activity, especially in the reduction of CO_2 [3–6]. The involvement of intermediates containing the radical anion $(N\text{–}N)^{\bullet-}$ in both the MLCT excited states, $[(N\text{–}N)^{\bullet-}Re^{II}(CO)_3X]^*$ [1,2], and in the electrocatalytic cycles [3,6] has prompted studies of the electrochemistry, spectroscopy [7] and spectroelectrochemistry (IR, UV–VIS, EPR) of systems $[(N\text{–}N)Re(CO)_3X]^{\bullet-}$ [8–12] with "18+δ" valence electron configuration [8a]. For reasons of symmetry and more sophisticated electronic structure we have also studied dinuclear systems $(\mu\text{-}N\text{–}N)[Re(CO)_3X]_2$ with corresponding bridging bis-bidentate ligands [7a,7b,13–15], among them the strongly π-accepting α-azoimine chelate system 2,2′-azobipyridine, abpy [7a,7b,16]. With X = Cl and Br these compounds could be well characterized and also studied by advanced computational methods [16]. Since the mononuclear series $(abpy)Re(CO)_3X$, X = F-I, was described previously [10], we have now investigated the dinuclear series $(\mu\text{-abpy})[Re(CO)_3X]_2$, X = F, Cl, Br or I. This report on possible structural alternatives (e.g. *syn*/*anti* isomerism), on the synthesis variation, on variable electrochemical behaviour, and on the spectroscopy (IR, UV–VIS, EPR at variable frequencies), particularly of the persistent radical forms $\{(\mu\text{-abpy})[Re(CO)_3X]_2\}^{\bullet-}$, will be discussed in connection with other dinuclear compounds of abpy [17] with electron-rich metals such as copper(I) [18], molybdenum(0) [19], tungsten(0) [20], ruthenium(II) [21], osmium(II) [22], rhodium(I) and iridium(II) [23].

The complexes $\{(\mu\text{-abpy})[Re(CO)_3Cl]_2\}^{o,-}$ and $\{(\mu\text{-abpy})[Re(CO)_3Br]_2\}^{o,-}$ have been reported earlier [7a,7b,9]. One purpose of this work was to obtain more precise information about the radical complexes by means of high-field/high-frequency EPR ($\nu \geqslant 200$ GHz). The series of complexes will also be extended to the new fluoride and iodide analogues. Few homodinuclear complexes with the metal complex fragment $[Re(CO)_3Br]$ are known, only one with $[Re(CO)_3I]$ [24] and none with $[Re(CO)_3F]$. To study the influence of the halide on $\{(\mu\text{-abpy})[Re(CO)_3X]_2\}^n$, the following methods have been employed: ^1H NMR, EPR (particularly high-field EPR), X-ray crystallography, cyclic voltammetry, UV/Vis and IR spectroelectrochemistry. Relevant DFT calculation results [16] will be used for discussion.

2. Syntheses and characterization

In comparison to the mononuclear systems $(abpy)Re(CO)_3X$ [10] the dinuclear complexes $\{(\mu\text{-abpy})[Re(CO)_3X]_2\}$ exhibit

* Corresponding author. Tel.: +49 711 68564170; fax: +49 711 68564165.
E-mail address: kaim@iac.uni-stuttgart.de (W. Kaim).

0022-328X/$ - see front matter © 2008 Elsevier B.V. All rights reserved.
doi:10.1016/j.jorganchem.2008.09.034

additional complications. They can occur as *syn* and *anti* isomers (Scheme 1), and reactions of two electron-rich precursors can lead to dinuclear radical anion complexes of abpy. This phenomenon has already been reported for rhodium and iridium complexes [23] as well as for copper compounds [25].

2.1. {(μ-abpy)[Re(CO)$_3$Br]$_2$} and {(μ-abpy)[Re(CO)$_3$I]$_2$}

The complex {(μ-abpy)[Re(CO)$_3$I]$_2$} was synthesized in the unreduced (neutral) state by the same route as the known chloride and bromide analogues [7a,7b]. While 4 h refluxing in a 3:1 toluene/dichloromethane mixture was sufficient for the synthesis of the chloride and bromide derivatives, 12 h were necessary to obtain the iodide complex.

Besides the elemental analysis (see Section 9) ^{1}H NMR spectroscopy was used for characterization. The isolated compound {(μ-abpy)[Re(CO)$_3$I]$_2$} showed a well-resolved spectrum for only one isomer with the expected [17] abpy coupling pattern (see Section 9). The complex {(μ-abpy)[Re(CO)$_3$Br]$_2$} exhibited a similar spectrum with slightly broadened signals, possibly due to traces of reduced material.

The ^{1}H NMR signals are slightly shifted to lower field with respect to the signals of the free ligand [7a,7b,9,17], they do not indicate clearly as to which of the possible *syn* or *anti* isomers are formed (see Section 3 below).

X band EPR showed that the isolated {(μ-abpy)[Re(CO)$_3$I]$_2$} does not involve a stable radical. It had to be reduced electrochemically to obtain an EPR signal at g_{iso} = 2.008 (see Section 7).

2.2. {(μ-abpy)[Re(CO)$_3$Cl]$_2$} and {(μ-abpy)[Re(CO)$_3$Cl]$_2$}$^{0/\bullet-}$

An alternative to the synthesis as shown in Scheme 1 for {(μ-abpy)[Re(CO)$_3$Cl]$_2$ is the reaction under refluxing conditions in toluene. The latter will be referred to as high-temperature synthesis (HT), whereas the procedure described in Scheme 1 will be referred to as low-temperature synthesis (LT).

The HT synthesis led to the formation of an EPR active material with g_{iso} = 2.004, which is the same value as obtained for the electrolytically reduced {(μ-abpy)[Re(CO)$_3$Cl]$_2$} as synthesized by the LT route. A well-resolved ^{1}H NMR spectrum could be obtained even for the radical compound, however, the compounds obtained from LT and HT syntheses exhibit different ^{1}H NMR shifts (see Section 9) although in both cases the expected coupling pattern of abpy is observed [7a,7b,9].

Elemental analyses confirm the {(μ-abpy)[Re(CO)$_3$Cl]$_2$} composition for both LT and HT products although the presence of a reduced radical form in the HT product requires a positive counter ion.

Mass spectrometry measurements using the FAB negative ion method showed that the expected isotope pattern is well reproduced for both LT and HT compounds.

2.3. {(μ-abpy)[Re(CO)$_3$F]$_2$}$^{0/\bullet-}$

For the fluoride-containing complex, a different route than in Scheme 1 was preferred (Scheme 2) since the precursor is not stable at higher temperatures.

Although it has been reported that Re(CO)$_5$F oligomerizes above room temperature [26], the reaction temperature had to be increased because no reaction took place below 55 °C. Since the chelating effect was believed to counteract the tendency of polymerization, that slight increase of temperature was hoped to have only a small effect on the synthesis. Not unexpectedly, however, the results obtained from elemental analyses were not satisfactory for {(μ-abpy)[Re(CO)$_3$F]$_2$} (Section 9). It was then discovered that the product displayed an intense EPR signal and that the percentage of the one-electron reduced form {(μ-abpy)[Re(CO)$_3$F]$_2$}$^{\bullet-}$ could be estimated to approximately 90% by polarography. Thus, a counter cation is required which would explain the deviation in the elemental analysis. Since the fluoride compound product did not crystallize we cannot as yet offer a suggestion of its full identity. It could be verified by IR spectroscopy that there is no other carbonyl containing moiety in the product ruling out the aggregation of the dinuclear complex with other Re(CO)$_n$ moieties [26].

In spite of the fact that the dinuclear fluoride complex is isolated predominantly as a stable radical, a moderately resolved ^{1}H NMR spectrum could be obtained (see Section 9). However, no information about possible isomers is provided by ^{1}H NMR spectroscopy. Conversely, cyclic voltammetry experiments (see Section 4) strongly suggest that *syn*/*anti* isomers are present.

Attempts to obtain {(μ-abpy)[Re(CO)$_3$F]$_2$} by exchanging bromide or iodide in corresponding species by fluoride were unsuccessful.

3. Crystal structures

A crystal structure of {(μ-abpy)[Re(CO)$_3$Cl]$_2$} has been reported [9]. Deep green crystals (needles) were obtained from a saturated solution of the HT synthesis product in acetone through layering with pentane. This material crystallized in the space group $P2_1/c$ and it was possible here to obtain the same structure [9] with

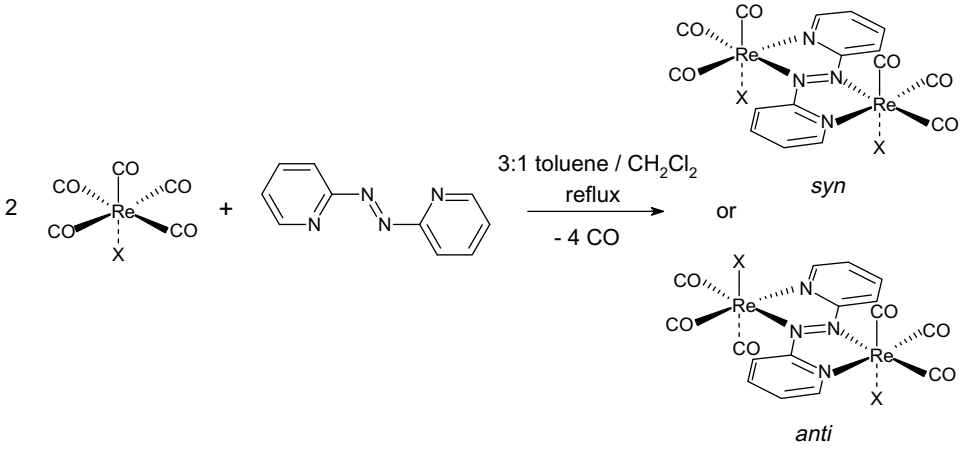

Scheme 1. Synthesis of {(μ-abpy)[Re(CO)$_3$X]$_2$}; X = Cl, Br, I.

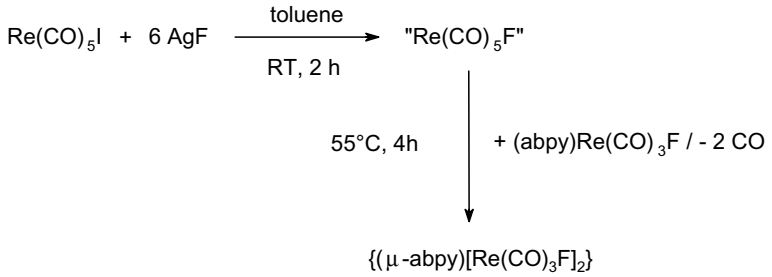

Scheme 2. Synthesis of $\{(\mu\text{-abpy})[Re(CO)_3F]_2\}^{o/\bullet-}$.

better *R* values. Green needles of $\{(\mu\text{-abpy})[Re(CO)_3Cl]_2\}$ for X-ray diffraction were obtained at room temperature by slow evaporation of a solution of $\{(\mu\text{-abpy})[Re(CO)_3Cl]_2\}$ (LT product) in dichloromethane, layered with hexane. Relevant crystallographic parameters for all structurally characterized species are presented in Table 1, selected bond lengths and angles are summarized in Tables 2 and 3. The packing of the unit cell is shown in Fig. 1 for the $P2_1/c$ form of $\{(\mu\text{-abpy})[Re(CO)_3Cl]_2\}$.

It was also possible to crystallize $\{(\mu\text{-abpy})[Re(CO)_3Cl]_2\}$ in another form, i.e. $I4_1/a$. This was obtained at room temperature by slow evaporation of a solution of $\{(\mu\text{-abpy})[Re(CO)_3Cl]_2\}$ (LT product) containing zinc dust (added for reduction purposes) in dichloromethane, layered with hexane. The packing of the unit cell is shown in Fig. 2.

No Zn^{2+} has been found in the structure, the crystal does not contain a radical (as shown e.g. by EPR measurements).

The packing in Fig. 2 shows two types of voids. In these voids there would be space for a small solvent molecule or a counter ion. However, no electron density of sufficiently quantity was found. The voids cause a drop in density from 2.512 g cm^{-3} ($P2_1/c$) to 2.228 g cm^{-3} ($I4_1/a$).

Table 2
Selected distances in Å for molecules $\{(\mu\text{-abpy})[Re(CO)_3X]_2\}$ (X = Cl, Br, I)

Compound	abpy [38]	X = Cl	X = Cl	X = Br	X = I
		$P2_1/c$	$I4_1/a$	$I4_1/a$	$C2/c$
N1–N1	1.246(2)	1.315(7)	1.314(8)	1.319(10)	1.308(8)
N1–Re	–	2.131(4)	2.119(4)	2.124(6)	2.123(7)
N2–Re	–	2.143(4)	2.134(5)	2.123(7)	2.130(4)
Re–X	–	2.4593(13)	2.4540(16)	2.5997(11)	2.7902(4)
Re–Re	–	5.034(8)	4.997(9)	5.023(11)	5.071(8)

The structure of crystallized $\{(\mu\text{-abpy})[Re(CO)_3Br]_2\}$ exhibits the same kind of packing as shown in Fig. 2. Thus, the new crystal form of $\{(\mu\text{-abpy})[Re(CO)_3Cl]_2\}$ and that of $\{(\mu\text{-abpy})[Re(CO)_3Br]_2\}$ are isostructural ($I4_1/a$). Green needles of $\{(\mu\text{-abpy})[Re(CO)_3Br]_2\}$ for X-ray diffraction were obtained at room temperature through slow evaporation of a solution of $\{(\mu\text{-abpy})[Re(CO)_3Br]_2\}$

Table 1
Crystallographic data of complexes

	$\{(\mu\text{-abpy})[Re(CO)_3Cl]_2\}$ 1st structure: $P2_1/c$	$\{(\mu\text{-abpy})[Re(CO)_3Cl]_2\}$ 2nd structure: $I4_1/a$	$\{(\mu\text{-abpy})[Re(CO)_3Br]_2\}$	$\{(\mu\text{-abpy})[Re(CO)_3I]_2\}$
Empirical formula	$C_{16}H_8Cl_2N_4O_6Re_2$	$C_{16}H_8Cl_2N_4O_6Re_2$	$C_{16}H_8Br_2N_4O_6Re_2$	$C_{16}H_8I_2N_4O_6Re_2$
Formula weight (g mol^{-1})	795.56	795.56	884.48	978.46
Crystal size (mm)	0.4 × 0.2 × 0.1	0.6 × 0.1 × 0.1	0.3 × 0.2 × 0.1	0.3 × 0.2 × 0.2
Temperature (K)	293(2)	293(2)	293(2)	293(2)
Wavelength (Å)	0.71073	0.71073	0.71073	0.71073
Crystal system	Monoclinic	Tetragonal	Tetragonal	Monoclinic
Space group	$P2_1/c$	$I4_1/a$	$I4_1/a$	$C2/c$
Unit cell dimensions				
a (Å)	6.44910(10)	25.2051(16)	25.5231(7)	15.2359(2)
b (Å)	11.9513(2)	25.2051(16)	25.5231(7)	10.7964(2)
c (Å)	13.7455(2)	7.4658(5)	7.5854(2)	13.7359(2)
β (°)	96.799(1)			104.866(1)
Cell volume (Å^3)	1051.99(3)	4743.0(5)	4941.3(2)	2183.83(6)
Calculated density (g cm^{-3})	2.512	2.228	2.378	2.976
Absorption coefficient (mm^{-1})	11.79	10.46	13.06	13.94
Maximum 2*θ* (°)	54.97	56.08	54.95	54.93
Index ranges	$-8 \leqslant h \leqslant 7$, $-15 \leqslant k \leqslant 15$, $-17 \leqslant l \leqslant 17$	$-33 \leqslant h \leqslant 33$, $-33 \leqslant k \leqslant 33$, $-9 \leqslant l \leqslant 9$	$-32 \leqslant h \leqslant 32$, $-32 \leqslant k \leqslant 32$, $-9 \leqslant l \leqslant 8$	$-19 \leqslant h \leqslant 19$, $-14 \leqslant k \leqslant 14$, $-17 \leqslant l \leqslant 17$
Formula units per cell, *Z*	2	8	8	4
Reflections collected	26000	22151	23329	25649
Unique reflections	2418	2797	2820	2498
R_{int}/R_σ	0.0964/0.0327	0.0660/0.0341	0.0849/0.0403	0.1236/0.0415
Goodnes-of-fit (GOF)/F^2	1.053	0.945	1.132	1.157
Data/restraints/parameters	2418/0/137	2797/0/153	2820/0/153	3598/0/137
R indices (for all data)	$R_1 = 0.0311$, $wR_2 = 0.0678$	$R_1 = 0.0438$, $wR_2 = 0.0756$	$R_1 = 0.0620$, $wR_2 = 0.1004$	$R_1 = 0.0326$, wR_2=0.0737
R indices (for $I > 2\sigma(I)$)	$R_1 = 0.0269$, $wR_2 = 0.0655$	$R_1 = 0.0304$, $wR_2 = 0.0719$	$R_1 = 0.0477$, $wR_2 = 0.0946$	$R_1 = 0.0303$, $wR_2 = 0.0725$
Extinction	0.0025(2)	0.00070(4)	0.00017(3)	0.00158(6)
Largest residual densities (e Å^{-3})	1.28, −1.15	0.98, −0.61	1.09, −1.13	1.46, −1.69

Table 3
Selected angles in ° for molecules {(μ-abpy)[Re(CO)$_3$X]$_2$} (X = Cl, Br, I)

	X = Cl	X = Cl	X = Br	X = I
	*P*21/*c*	*I*4$_1$/*a*	*I*4$_1$/*a*	*C*2/*c*
C1–Re–C2	89.3(2)	90.1(3)	89.3(4)	91.8(2)
C1–Re–C3	92.2(2)	91.1(3)	91.2(4)	89.8(2)
O1–C1–Re	177.4(5)	177.9(6)	179.4(8)	175.8(5)
O2–C2–Re	178.4(5)	175.3(6)	175.0(10)	179.4(6)
O3–C3–Re	176.3(5)	175.9(2)	176.1(11)	176.8(5)
C1–Re–X	178.5(2)	177.9(2)	177.6(3)	175.99(17)
C2–Re–X	91.98(18)	90.6(9)	90.9(3)	91.69(18)
C3–Re–X	87.17(16)	86.9(2)	86.4(3)	88.60(16)
N1–Re–X	85.75(10)	86.53(12)	85.99(17)	85.42(10)
N2–Re–X	82.33(10)	81.75(12)	82.10(18)	85.12(11)
C1–Re–N1	93.04(19)	93.2(2)	94.3(3)	91.45(19)
C2–Re–N2	98.24(19)	95.3(2)	95.2(3)	96.1(2)

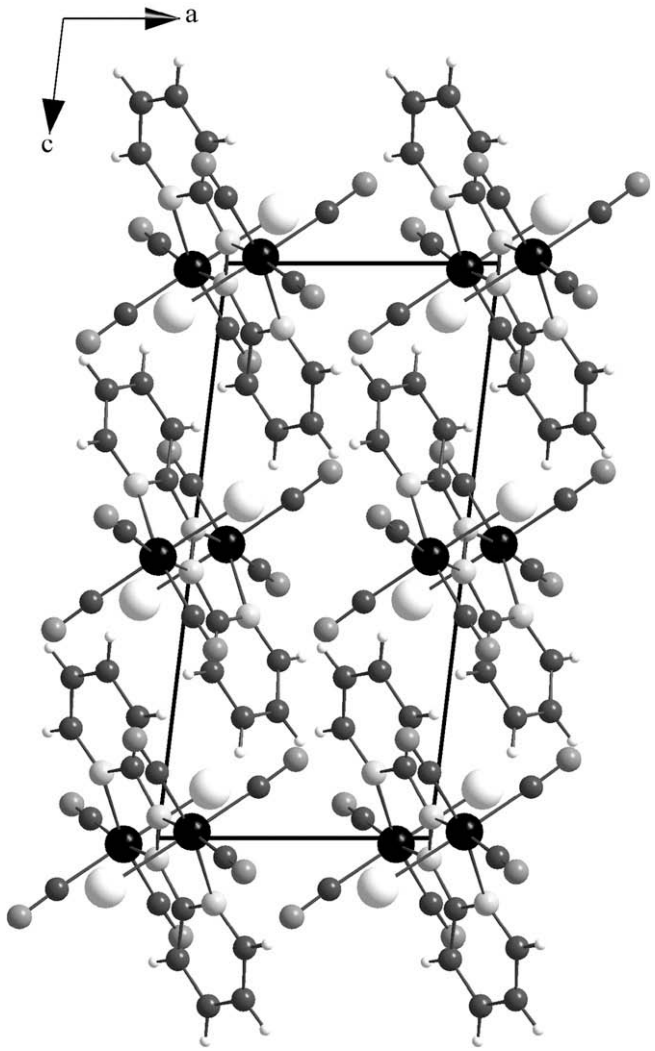

Fig. 1. Arrangement of {(μ-abpy)[Re(CO)$_3$Cl]$_2$} in the unit cell (*P*2$_1$/*c*).

containing Zn dust (added for reduction purposes) in dichloromethane, layered with hexane. A crystal of {(μ-abpy)[Re(CO)$_3$Cl]$_2$} obtained by the high-temperature synthesis to yield a paramagnetic solution (shown by EPR) gave the same *I*4$_1$/*a* structure. It may be assumed that the tetragonal crystals require the radical anion form for nucleation but that the diamagnetic neutral forms have a higher crystallizing rate and a lower solubility in common organic solvents.

Single crystals of {(μ-abpy)[Re(CO)$_3$I]$_2$} were obtained from a non-reduced solution of the complex, which crystallizes in *C*2/*c*. Green needles for X-ray diffraction were obtained at room temperature through slow evaporation of a solution in acetone, layered with hexane. The packing of the unit cell is shown in Fig. 3.

The molecular structures of the complexes {(μ-abpy)[Re(CO)$_3$X]$_2$} (X = Cl, Br, I) are given in Figs. 4 and 5. All structures exhibit centers of inversion for the molecules. Little change is observed in the overall molecular arrangement on going from the chloride to the iodide complexes. All structures show the (s-*cis*)-*E*-(s-*cis*) conformation of the approximately planar abpy bridge (see below) and an *anti* arrangement of the halides with respect to the abpy ligand plane.

The azo bond length (N1–N1) is not significantly influenced by the change of the halogen (Table 2). The N1–N1 distance is lengthened relative to that in the free ligand value due to both steric effects (induced by the coordination of two heavy atoms) and by electronic factors such as π back donation. Even though the solutions from which the *I*4$_1$/*a* compounds were crystallized contained radicals as shown by EPR measurements, the crystals did not show EPR signals and the structures do not involve a reduced compound. In fact, the azo bond lengths at ca. 1.31 Å would be short for one-electron reduced abpy [28]. From calculations on {(μ-abpy)[Re(CO)$_3$Cl]$_2$}^{n} [16], the bond length should increase from 1.329 Å for the neutral complex ($n = 0$) to 1.359 Å for the stable radical anion ($n = -1$). This has been confirmed experimentally by the example of the *abcp* complex {(μ-abcp)[Cu(PPh$_3$)$_2$]$_2$}(PF$_6$), abcp = 2,2′-azobis(5-chloropyrimidine), [29] with an azo N–N bond length at 1.345 Å.

It is noteworthy that all rhenium–nitrogen bond lengths are similar despite different halide substituents, X, and different nitrogen atoms (π accepting azo N and basic pyridyl N). The comparable distances Re^I–N$_{azo}$ and Re^I–N$_{pyridyl}$ reflect a compensation of π back bonding and σ donor effects for both kinds of N donor centers. Similarly, the increasing halogen size in the series Cl < Br < I may be compensated by increasingly covalent binding to the metal.

The Re–Re distances across the compact abpy bridge are also of interest. The rhenium–rhenium distance is slightly longer for the iodide complex (Table 2). The reason lies in the more planar conformation of the bridge in the iodide compound. In fact, the dihedral angles between the N1–Re–N2 plane and the pyridyl ring plane are 11.5° for the iodide complex whereas they are 21.3° for the bromide and 21.5° and 23.1° for the *P*2$_1$/*c* and *I*4$_1$/*a* forms of the chloride, respectively.

Regarding the bond angles (Table 3) there are very few differences between the analogues. The largest deviation is observed for {(μ-abpy)[Re(CO)$_3$I]$_2$} in which the angles O1–C1–Re and C1–Re–X are smaller by about 2–3° in comparison to the other analogues. This cannot be induced by I$^-$/I$^-$ interactions since the smallest I–I distances are about 5 Å. The halide/rhenium/*trans*-CO alignment is thus less linear for {(μ-abpy)[Re(CO)$_3$I]$_2$} than for the chloride and bromide complexes, which has also been observed for (abpy)Re(CO)$_3$I in the mononuclear series [10] and may be explained by the better electron donor effect of I$^-$.

4. Cyclic voltammetry

The new dinuclear complexes {(μ-abpy)[Re(CO)$_3$F]$_2$}$^{o/\bullet-}$ and {(μ-abpy)[Re(CO)$_3$I]$_2$} as well as the high-temperature product {(μ-abpy)[Re(CO)$_3$Cl]$_2$}$^{o/\bullet-}$ will be separately described with respect to their redox behavior. The potentials obtained for these three compounds are summarized in Table 4.

The isomerically uniform compound *anti*-{(μ-abpy)[Re(CO)$_3$I]$_2$} exhibits a typical electrochemical behavior upon reduction (Fig. 6) as observed previously for {(μ-abpy)[Re(CO)$_3$Cl]$_2$} and {(μ-abpy)[Re(CO)$_3$Br]$_2$} [7a,7b,9].

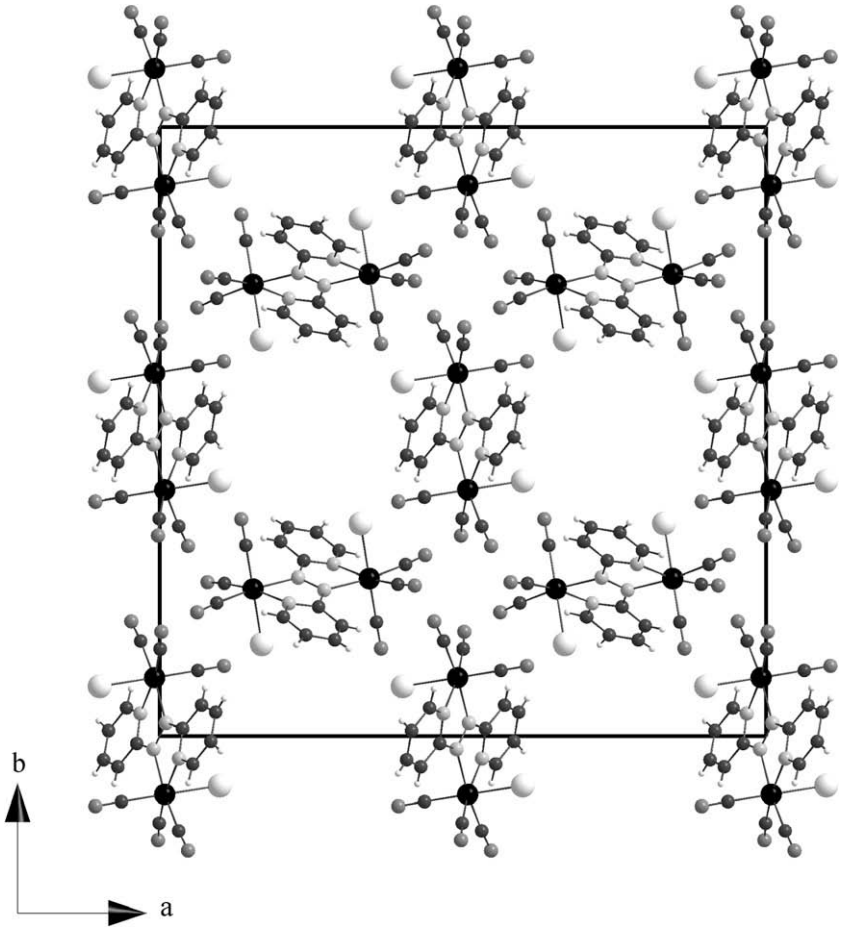

Fig. 2. Packing of {(μ-abpy)[Re(CO)$_3$Cl]$_2$} molecules in the unit cell ($I4_1/a$); {(μ-abpy)[Re(CO)$_3$Br]$_2$} is isostructural.

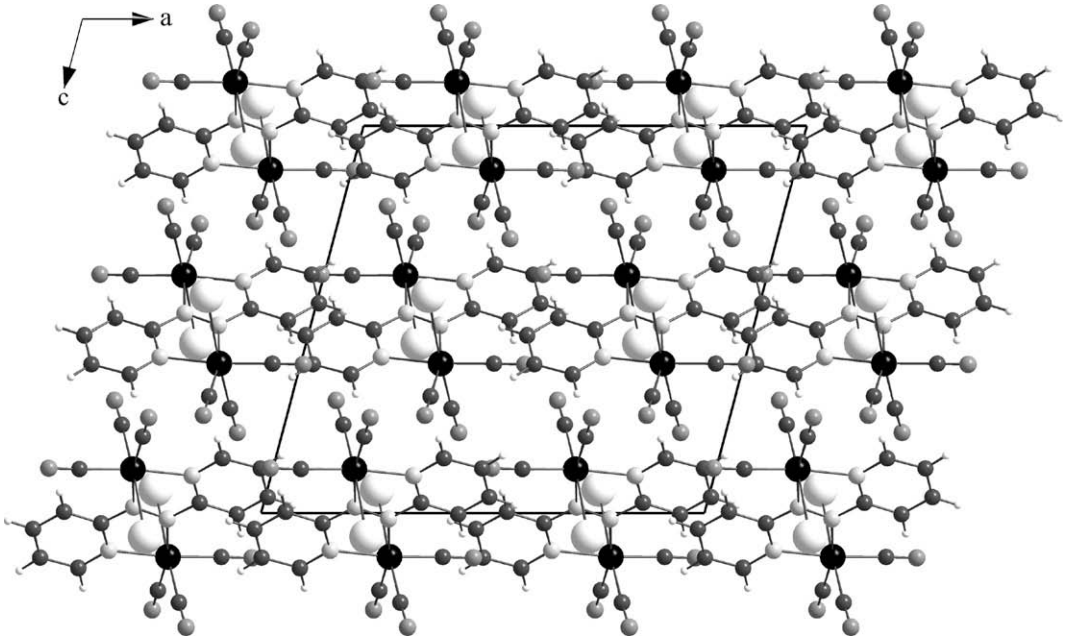

Fig. 3. Arrangement of {(μ-abpy)[Re(CO)$_3$I]$_2$} molecules in the unit cell ($C2/c$).

The first reduction step occurs in a totally reversible fashion, involving an azo-centered reduction (see below). The chloride and bromide analogues have similar reduction potentials, whereas the iodide complex is slightly less easy to reduce. The chloride and bromide complexes also display the same potential for the second reduction which is not an entirely reversible process. This step

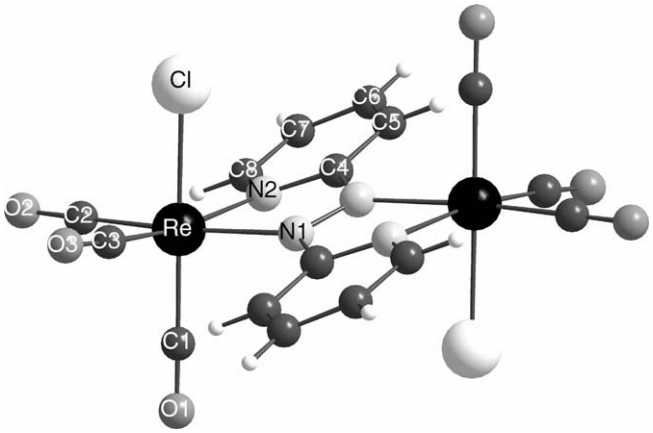

Fig. 4. Molecular structure of $\{(\mu\text{-abpy})[Re(CO)_3Cl]_2\}$ in the crystal ($I4_1/a$); $\{(\mu\text{-abpy})[Re(CO)_3Br]_2\}$ is isostructural.

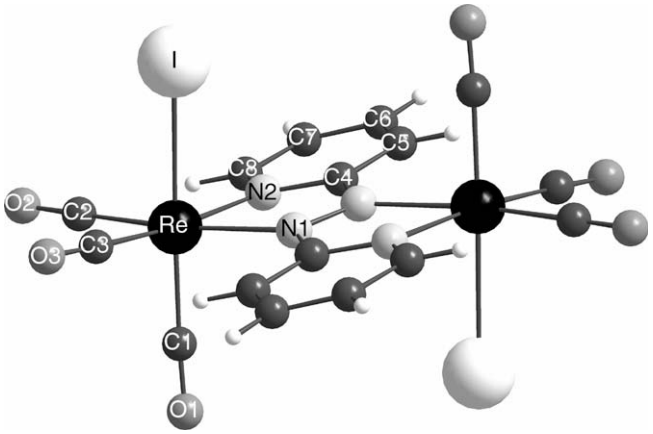

Fig. 5. Molecular structure of $\{(\mu\text{-abpy})[Re(CO)_3I]_2\}$ in the crystal ($C2/c$).

consists of the uptake of a second electron followed by the slow loss of a halide. The $|E_2–E_1|$ values point to a slightly easier release of the halide for the iodide complex. The loss of the halide appears to be less dependent on the halogen variation in the case of the dinuclear complexes than for the mononuclear complexes [10]. This can be rationalized by the less negative reduction potentials in the case of the dinuclear systems.

Table 4
Electrochemical potentials[a] from cyclic voltammetry[b]

Complex	E_1[c]	E_2[d]	$\lvert E_2–E_1\rvert$
$\{(\mu\text{-abpy})[Re(CO)_3F]_2\}$[e]	0.36	−0.84	0.48
	0.53[f]	−0.63[f]	1.16
$\{(\mu\text{-abpy})[Re(CO)_3Cl]_2\}$[e]	0.00	−0.81	0.81
	0.28[f]	−0.58[f]	0.86
$\{(\mu\text{-abpy})[Re(CO)_3Cl]_2\}$ [7a,7b][e]	−0.01	−0.81	0.80
$\{(\mu\text{-abpy})[Re(CO)_3Br]_2\}$ [7a,7b][g]	−0.02	−0.81	0.79
$\{(\mu\text{-abpy})[Re(CO)_3I]_2\}$[e]	−0.10	−0.86	0.76

[a] Potentials E in V vs. $FeCp_2^{0/+}$.
[b] At 100 mV/s scan rate.
[c] Half-wave potential corresponding to a reversible step.
[d] Half-wave potential corresponding to a quasi-reversible step (peak current ratio <1).
[e] Measurements in CH_2Cl_2/0.1 M Bu_4NPF_6.
[f] Attributed to syn isomer, all other potentials refer to the *anti* isomer.
[g] Measurements in DCE/0.1 M Bu_4NPF_6 vs. SCE, conversion according to the literature values [73].

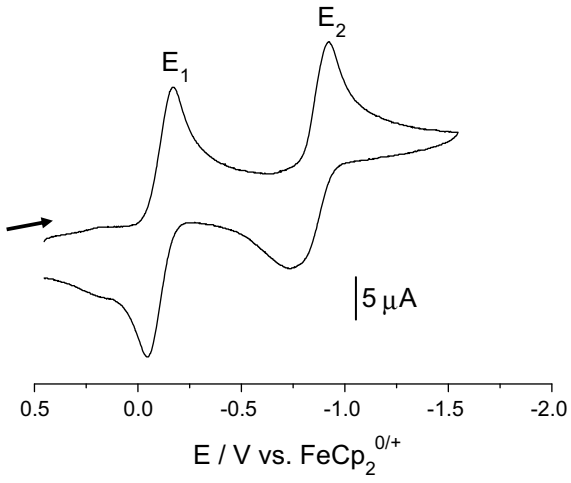

Fig. 6. Cyclic voltammogram of $\{(\mu\text{-abpy})[Re(CO)_3I]_2\}$ in CH_2Cl_2/0.1 M Bu_4NPF_6 (scan rate: 100 mV/s).

The product $\{(\mu\text{-abpy})[Re(CO)_3Cl]_2\}^{o/\bullet-}$ obtained by high-temperature synthesis (see Section 2) exhibits a different electrochemical behavior than the previously described compounds $\{(\mu\text{-abpy})[Re(CO)_3X]_2\}$ (X = Cl, Br, I). In the cyclic voltammogram two waves at $E_1 = 0.28$ V vs. $FeCp_2^{0/+}$ [30] and at $E_{1'} = 0.00$ V are fully reversible and may thus represent two isomers (*syn*/*anti*, ca. 45% reduced at E_1 and 55% at $E_{1'}$). Two irreversible waves at $E_2 = -0.58$ V and $E_{2'} = -0.81$ V would then reflect the second reduction with the first chloride dissociation [10]. At $E_3 = -1.10$ V vs. $FeCp_2^{0/+}$ another reversible wave of higher intensity is observed which concerns a species with one less chloride ligand (no isomers possible).

The complex $\{(\mu\text{-abpy})[Re(CO)_3F]_2\}^{o/\bullet-}$ exhibits an electrochemical behavior which is similar to that of $\{(\mu\text{-abpy})[Re(CO)_3Cl]_2\}^{o/\bullet-}$ (HT product). Polarographic measurements with a mercury electrode have established that the compound studied was a mixture of approximately 90% of reduced species and 10% of the neutral form. Thus, in order to obtain proper voltammograms, the compound had to be polarized first, either totally reduced to $\{[(\mu\text{-abpy})Re(CO)_3F]_2\}^{\bullet-}$, or fully oxidized to $\{[(\mu\text{-abpy})Re(CO)_3F]_2\}$. It was preferred to oxidize it (Fig. 7) for better comparison.

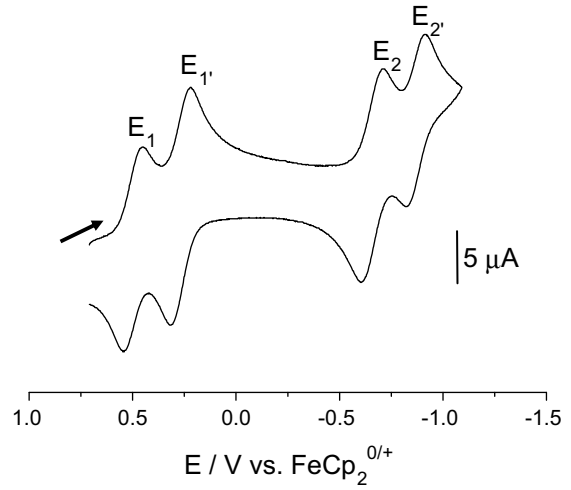

Fig. 7. Cyclic voltammogram of $\{(\mu\text{-abpy})[Re(CO)_3F]_2\}$ in CH_2Cl_2/0.1 M Bu_4NPF_6 (scan rate: 100 mV/s).

The cyclic voltammogram shows four signals of comparable intensity which can be grouped into two sets of two signals. This points again to the presence of a *syn/anti* isomer mixture in the compound which was originally isolated in 90% reduced and thus Re–F bond-labilized form. From the current ratio it appears that ca. 45% of the neutral complex is reduced at E_1 and ca. 55% at $E_{1'}$ (*syn*/*anti* isomers). These steps are totally reversible, they can be assigned to abpy centered reductions which occur at very positive potentials, about 0.3 V higher than for the chloride system. The reduction potentials thus vary from about +0.45 V (fluoride complex, 90% reduced form isolated) via −0.0 V (chloride complex, containing only small amounts of reduced form) to −0.10 V vs. $FeCp_2^{0/+}$ (iodide complex, no reduced form isolated). This series nicely illustrates how the formation of anion radicals during synthesis correlates with the reduction potential.

Upon uptake of a second electron, that sequence seems to be inverted. This step involves an EC mechanism where loss of the halide takes place after second reduction. This release of halide appears to occur as easily for the fluoride compound at E_2 and $E_{2'}$ as for the chloride analogue.

5. UV/Vis spectroelectrochemistry

The complexes {(μ-abpy)[Re(CO)$_3$Cl]$_2$} (low-temperature product), {(μ-abpy)[Re(CO)$_3$Br]$_2$} and {(μ-abpy)[Re(CO)$_3$I]$_2$} exhibit similar spectroelectrochemical behavior as shown in Table 5 and as illustrated by Fig. 8 for {(μ-abpy)[Re(CO)$_3$I]$_2$}.

The neutral complexes {(μ-abpy)[Re(CO)$_3$X]$_2$} exhibit long-wavelength metal-to-ligand charge transfer (MLCT) bands at about 800 nm with high- and low-energy shoulders [7a,7b]. The bands at about 400 nm can also be assigned to MLCT transitions ($d\rightarrow\pi_2^*$ (abpy) [7b]).

On reversible one-electron reduction the complexes {(μ-abpy)[Re(CO)$_3$X]$_2$} exhibit the expected high-energy shift and intensity reduction of the MLCT band to about 650 nm. They also display the typical intra-ligand bands of azoaromatic radical anions at about 390 and 500 nm, as shown also in Table 5 for abpy$^{\bullet-}$.

After the second reduction the MLCT ($d\rightarrow\pi_1^*$(abpy)) band vanishes and structured bands at ca. 500 nm appear which are tentatively assigned to ligand (abpy^{2-})-to-metal transitions (LMCT).

The complexes {(μ-abpy)[Re(CO)$_3$F]$_2$}$^{o/\bullet-}$ and {(μ-abpy)[Re(CO)$_3$Cl]$_2$}$^{o/\bullet-}$ which exhibit comparable electrochemical behavior as shown in Section 4 were compared by means of UV/Vis spectroelectrochemistry (Table 6).

Table 5
Absorption data obtained from spectroelectrochemistry in CH_2Cl_2/0.1 M Bu_4NPF_6

Compound	λ_{max}/nm (ε/103 M^{-1} cm^{-1})
abpy [21][a]	312(8.7), 470(0.9)
abpy$^{\bullet-}$ [21][a]	286sh, 360sh, 408(26.5), 548(2.6)
abpy^{2-} [21][a]	275sh, 342sh, 358(14.2), 380sh, 450sh
{(μ-abpy)[Re(CO)$_3$Cl]$_2$}	331(9.7), 412(10.3), 590sh, 705sh, 784(11.0)
{(μ-abpy)[Re(CO)$_3$Cl]$_2$}$^{\bullet-}$	310sh, 383(11.2), 496(7.4), 615(5.7)
[(CO)$_3$Re(μ-abpy)Re(CO)$_3$Cl]$^-$	329(10.7), 396(7.1), 481(8.0), 506(8.1), 550sh, 735(3.1)
{(μ-abpy)[Re(CO)$_3$Br]$_2$}	334(12.4), 395(14.4), 700sh, 795(5.0)
{(μ-abpy)[Re(CO)$_3$Br]$_2$}$^{\bullet-}$	335(11.4), 387(11.4), 460sh, 505(8.4), 540sh, 645(5.0)
[(CO)$_3$Re(μ-abpy)Re(CO)$_3$Br]$^-$	329(12.4), 400sh, 483(9.4), 505(9.4), 540sh, 713(2.0)
{(μ-abpy)[Re(CO)$_3$I]$_2$}	355(8.2), 397(8.2), 421(6.6), 488(3.6), 735sh, 826(5.3)
{(μ-abpy)[Re(CO)$_3$I]$_2$}$^{\bullet-}$	355(8.2), 376(8.0), 508(4.9), 545sh, 660(2.5)
[(CO)$_3$Re(μ-abpy)Re(CO)$_3$I]$^-$	320sh, 470(5.8), 500(6.0), 535sh

[a] Measurements in DMF/0.1 M Bu_4NPF_6.

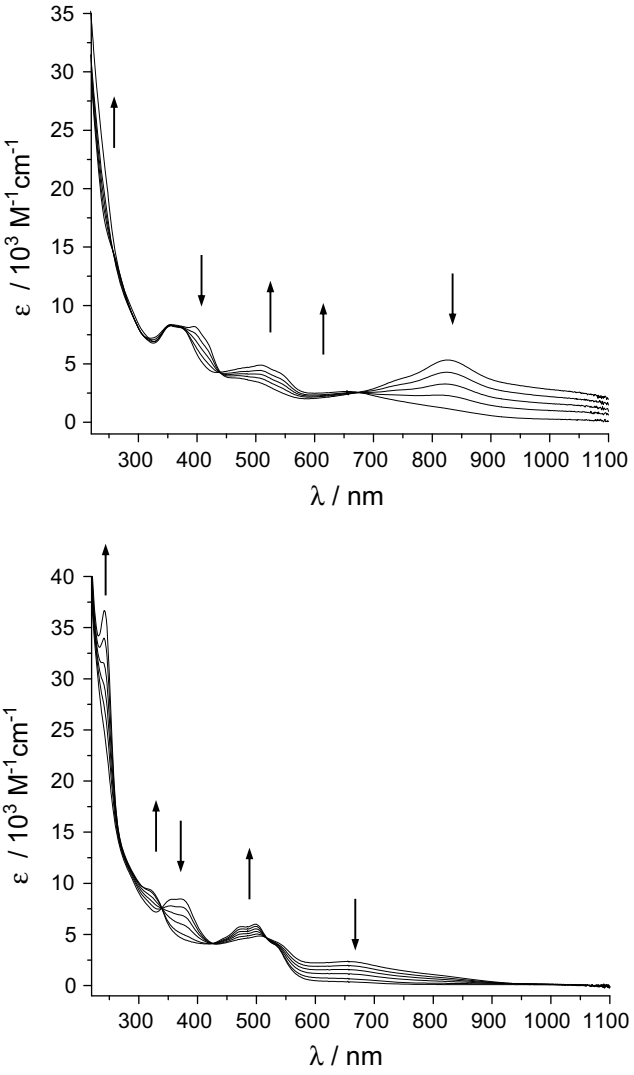

Fig. 8. UV–Vis-spectroelectrochemical reduction at E_1 (top) and E_2 (bottom) from {(μ-abpy)[Re(CO)$_3$I]$_2$} via the radical anion to [(CO)$_3$Re(μ-abpy)Re(CO)$_3$I]$^-$ in CH_2Cl_2/0.1 M Bu_4NPF_6.

Table 6
Absorption data[a] obtained from spectroelectrochemistry in CH_2Cl_2/0.1 M Bu_4NPF_6 for {(μ-abpy)[Re(CO)$_3$X]$_2$}$^{o/\bullet-}$ (X = F, Cl)

Compound	λ_{max}/nm (ε/103 M^{-1} cm^{-1})
{(μ-abpy)[Re(CO)$_3$F]$_2$}	275sh, 340sh, 425(0.59), 700(0.59)
{(μ-abpy)[Re(CO)$_3$F]$_2$}$^{\bullet-}$ at E_1	280sh, 340sh, 350sh, 423(0.47), 510sh, 706(0.35)
{(μ-abpy)[Re(CO)$_3$F]$_2$}$^{\bullet-}$ at $E_{1'}$	275sh, 350(0.45), 380sh, 455(0.34), 480sh, 520sh, 620sh
{[(CO)$_3$Re](μ-abpy)[Re(CO)$_3$F]$_2$}– at E_2	240sh, 380(0.35), 440sh, 471(0.35), 496(0.36), 530sh, 630sh
{[(CO)$_3$Re](μ-abpy)[Re(CO)$_3$F]$_2$}– at $E_{2'}$	240sh, 330sh, 440sh, 471(0.36), 498(0.35), 535sh
{(μ-abpy)[Re(CO)$_3$Cl]$_2$}	281(0.76), 405(0.42), 588(0.29), 747(0.27)
{(μ-abpy)[Re(CO)$_3$Cl]$_2$}$^{\bullet-}$ at E_1	281(0.76), 380(0.49), 582(0.31), 730sh
{(μ-abpy)[Re(CO)$_3$Cl]$_2$}$^{\bullet-}$ at $E_{1'}$	268(0.84), 370(0.37), 582(0.20)
{[(CO)$_3$Re](μ-abpy)[Re(CO)$_3$Cl]$_2$}$^-$ at E_2	270sh, 368(0.37), 670sh
{[(CO)$_3$Re](μ-abpy)[Re(CO)$_3$Cl]$_2$}– at $E_{2'}$	275sh, 320sh, 466(0.33), 502(0.31), 540sh

Measurements in DMF/0.1 M Bu_4NPF_6.

[a] Molar extinction coefficients are not given for the complexes since the precise formulae including the counter ion are not known for the partially radical complexes. Absorbance values are given (in italics) for comparison purposes between the different steps.

The spectroelectrochemical series appear as two steps despite the occurrence of four waves in cyclic voltammetry since *syn/anti* isomers are not expected to exhibit very different spectra. The features observed on reduction (E_1 and $E_{1'}$ together as well as E_2 and $E_{2'}$) are in agreement with the results observed for the other halide complexes (Table 6).

For the neutral species the bands at around 700–800 nm, assigned to MLCT transitions, show the opposite trend to what might be expected from the electrochemical values, the lower reduction potential suggesting a higher π^* orbital for the iodide. This apparent discrepancy can be explained by a strong destabilization of d_{Re} while going from fluoride to iodide. The bands around 400 nm are tentatively assigned to the second MLCT process.

The monoreduced species exhibit MLCT bands at 600–660 nm. The trend observed is the same as for the neutral species. However, as expected, the absorptions are all shifted to higher energies, due to the decreased π acceptor capability of abpy$^{\bullet-}$ with respect to abpy. The bands at ca. 500 nm and 380 nm are typical IL bands for abpy$^{\bullet-}$ complexes (for abpy$^{\bullet-}$, bands are at 548 and 408 nm [17]). The species obtained after the second reduction exhibit structured bands at ca. 500 nm.

6. IR spectroelectrochemistry

The complexes {(μ-abpy)[Re(CO)$_3$Cl]$_2$} (low-temperature product), {(μ-abpy)[Re(CO)$_3$Br]$_2$} and {(μ-abpy)[Re(CO)$_3$I]$_2$} exhibit similar behavior as shown in Table 7 and as illustrated in Fig. 9 for {(μ-abpy)[Re(CO)$_3$I]$_2$}. The carbonyl stretching in the Re(CO)$_3$Cl fragment and the ring vibrations from the pyridyl moieties of the ligand were monitored.

The neutral complexes {(μ-abpy)[Re(CO)$_3$X]$_2$} display the expected three-band pattern for *fac*-Re(CO)$_3$ moieties with asymmetrical co-ligation. No relevant changes are observed while going from the chloride to the iodide complex.

The dinuclear complexes exhibit a similar behavior on reduction as the mononuclear complexes [10]. After one-electron reduction the expected low-energy shift of the carbonyl stretching bands is observed for all complexes while no change is observed in the pyridyl ring vibrations.

The shifts observed after the second reduction are less pronounced than those recorded for the first reduction. This can be explained by the fact that there is no change of charge due to the loss of one halide. Accordingly, the narrow high-energy CO stretching bands show a clear splitting because of the asymmetry of [(CO)$_3$Re(μ-abpy)Re(CO)$_3$X]$^-$. It is noteworthy that the bands for the pyridyl ring vibrations at about 1600 and 1470 cm^{-1} become more intense (Fig. 9). This suggests that the inversion symmetry is lost, caused by the dissociation of one halide: According to IR spectroscopy selection rules the transition must be accompanied by a change in the dipole moment to produce well observable bands. The normally split low-energy CO stretching bands merge into one broad feature due to the overlap of four closely spaced bands. Again, no significant variations of the stretching frequencies are observed upon going from chloride to iodide.

It has been shown from the electrochemical and UV/Vis spectroelectrochemical measurements that the complexes {(μ-abpy)[Re(CO)$_3$F]$_2$}$^{o/\bullet-}$ and {(μ-abpy)[Re(CO)$_3$Cl]$_2$}$^{o/\bullet-}$ exhibit comparable behavior. Thus, they will also be compared by means of IR spectroelectrochemistry in the carbonyl stretching and the pyridyl ring vibration regions. The spectral changes are shown by the example of {(μ-abpy)[Re(CO)$_3$F]$_2$}$^{\bullet-}$ in Figs. 10 and 11, the values are summarized in Table 8.

The electrochemically generated neutral complexes {(μ-abpy)[Re(CO)$_3$X]$_2$} exhibit again the expected three-band pattern. The broadening of the bands and the shoulders observed (for all states) can be explained by the presence of *syn/anti* isomers. After the first reduction more than three bands are observed. The non-reduced form of one isomer remains while the easier reducible other isomer is being converted.

The neutral fluoride and chloride complexes exhibit similar stretching frequencies. The values obtained for {(μ-abpy)[Re(CO)$_3$Cl]$_2$}$^{\bullet-}$ (HT product) are significantly different from the values obtained for *anti*-{(μ-abpy)[Re(CO)$_3$Cl]$_2$}$^{\bullet-}$ as electro-

Table 7
IR vibrational data obtained from spectroelectrochemistry in CH_2Cl_2/0.1 M Bu_4NPF_6 for {(μ-abpy)[Re(CO)$_3$X]$_2$} (X=Cl, Br, I)

Complex	$\tilde{\nu}_{CO}$/cm^{-1}		
{(μ-abpy)[Re(CO)$_3$Cl]$_2$}	2012(vs)	1953(s)	1939(s)
{(μ-abpy)[Re(CO)$_3$Cl]$_2$}$^{\bullet-}$	2012sh, 2007(vs)	1912(s)	1894sh
[(CO)$_3$Re(μ-abpy)Re(CO)$_3$Cl]$^-$	2001(s)/1991(s)	1882(s),br	
{(μ-abpy)[Re(CO)$_3$Br]$_2$}	2046sh, 2014 (vs)	1959(s)	1941(s)
{(μ-abpy)[Re(CO)$_3$Br]$_2$}$^{\bullet-}$	2014sh, 2008(vs)	1912(s)	1899(b)
[(CO)$_3$Re(μ-abpy)Re(CO)$_3$Br]$^-$	2001(s)/1992(s)	1883(s),br	
{(μ-abpy)[Re(CO)$_3$I]$_2$}	2042sh, 2012(vs)	1953(s)	1938(s)
{(μ-abpy)[Re(CO)$_3$I]$_2$}$^{\bullet-}$	2012sh, 2005(vs)	1907(s)	1897sh
[(CO)$_3$Re(μ-abpy)Re(CO)$_3$I]$^-$	1999(s)/1990sh	1881(s),br	

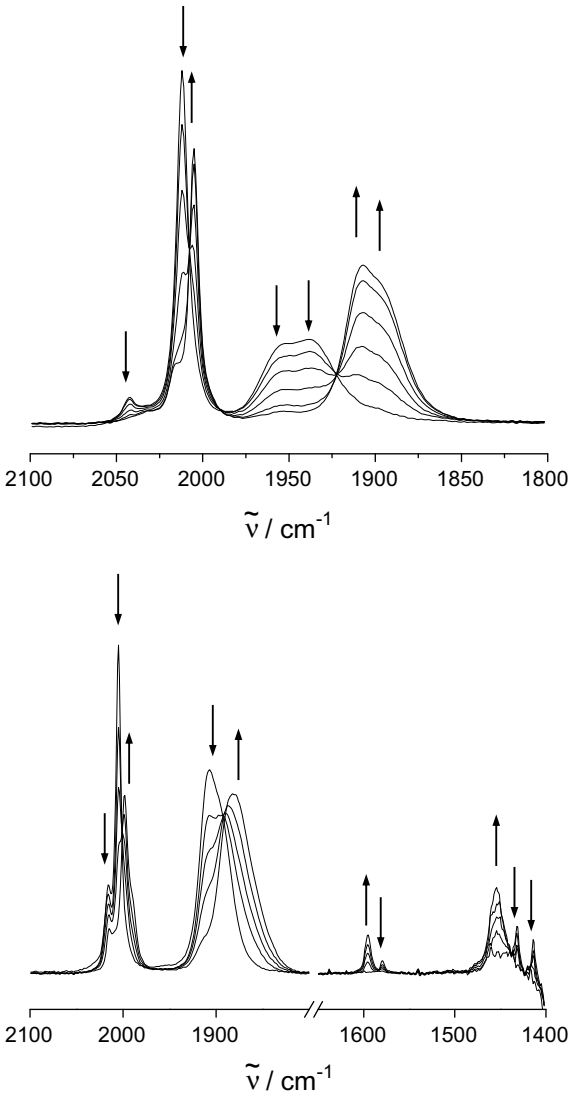

Fig. 9. IR-spectroelectrochemical reduction at E_1 (top) and E_2 (bottom) from {(μ-abpy)[Re(CO)$_3$I]$_2$} via the radical anion to [(CO)$_3$Re(μ-abpy)Re(CO)$_3$I]$^-$ in CH_2Cl_2/0.1 M Bu_4NPF_6.

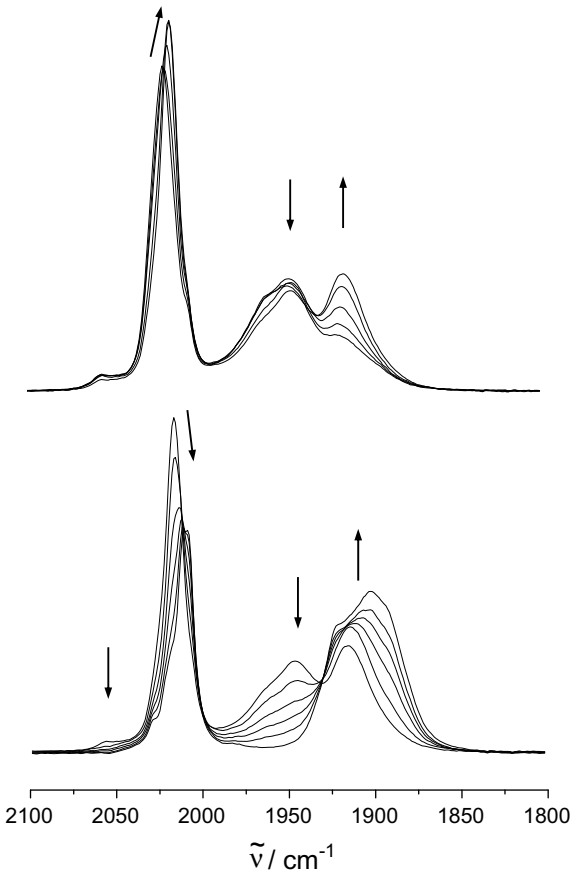

Fig. 10. IR-spectroelectrochemical reduction at E_1 (top) and $E_{1'}$ (bottom) of {(μ-abpy)[Re(CO)$_3$F]$_2$} to {(μ-abpy)[Re(CO)$_3$F]$_2$}$^{\bullet-}$ in CH_2Cl_2/0.1 M Bu_4NPF_6.

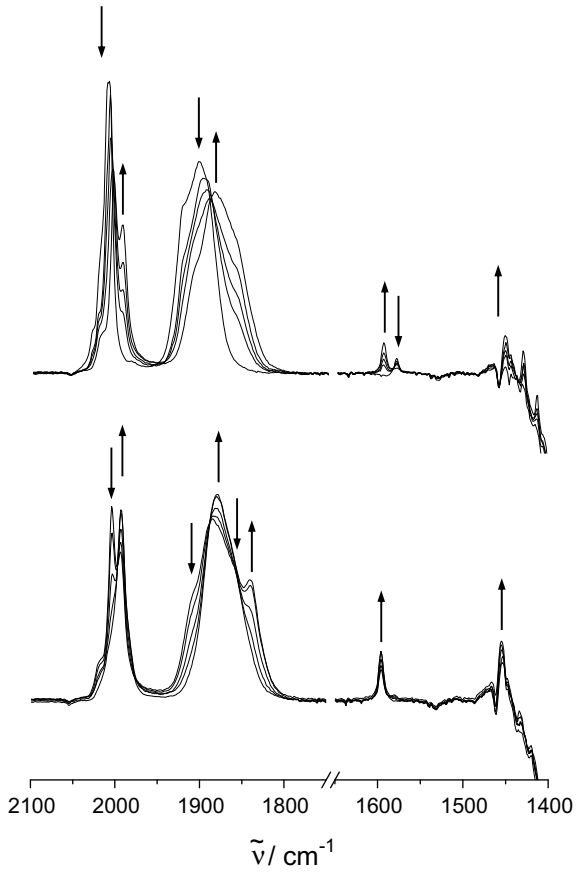

Fig. 11. IR-spectroelectrochemical reduction at E_2 (top) and $E_{2'}$ (bottom) from {(μ-abpy)[Re(CO)$_3$F]$_2$}$^{\bullet-}$ to {[(CO)$_3$Re](μ-abpy)[Re(CO)$_3$F]}$^-$ in CH_2Cl_2/0.1 M Bu_4NPF_6.

generated from the LT product. This shows that there are isomers in case of the HT product (which contains some stable radical) but not in the case of the LT form.

On the first and second reduction steps at E_1 and $E_{1'}$, the expected low-energy shifts for the carbonyl stretching bands are observed (Fig. 10). No intense ring vibration IR bands are displayed during these steps, confirming that they are associated with the first reduction processes of two isomers.

The spectra displayed on the third and fourth reductions at E_2 and $E_{2'}$ correspond to the features expected for an EC mechanism where one of the halide is dissociated. The shifts observed after these second reduction processes are less pronounced than those recorded for the first reductions. This can be explained by the fact that there is no change of charge due to the loss of one halide. Accordingly, the narrow high-energy CO stretching bands show a clear splitting because of the asymmetry of [(CO)$_3$Re(μ-abpy)Re(CO)$_3$X]$^-$. It is noteworthy that the bands for the pyridyl ring vibrations at about 1600 and 1470 cm^{-1} become more intense (Fig. 11). This suggests that the inversion symmetry is lost, caused by the dissociation of one halide.

Table 8
IR vibrational data obtained from spectroelectrochemistry in CH_2Cl_2/0.1 M Bu_4NPF_6 of {(μ-abpy)[Re(CO)$_3$X]$_2$}$^{o/\bullet-}$ (X = F, Cl)

Complex	$\tilde{\nu}_{CO}$/cm^{-1}		
{(μ-abpy)[Re(CO)$_3$F]$_2$}	2056sh	1960sh	1918(s)
	2020(vs)	1948(s)	
	2006sh		
{(μ-abpy)[Re(CO)$_3$F]$_2$}$^{\bullet-}$ at E_1	2056sh	1965sh	1916(s)
	2017(s)	1946(s)	
{(μ-abpy)[Re(CO)$_3$F]2}$^{\bullet-}$ at $E_{1'}$	2019sh	1921(s)	1903(s)
	2009(s)		1892sh
[(CO)$_3$Re(μ-abpy)Re(CO)$_3$F]$^-$ at E_2	2004(s)/1993(s)	1910sh	
	2020sh	1886(s),br	
		1860sh	
[(CO)$_3$Re(μ-abpy)Re(CO)$_3$F]$^-$ at $E_{2'}$	2009sh	1878(s),br	1838(s)
	1992(s)	1862sh	
{(μ-abpy)[Re(CO)$_3$Cl]$_2$}	2035sh/2023(s)	1961sh	
	2012(s)/1999sh	1940sh	
		1919(s),br	
{(μ-abpy)[Re(CO)$_3$Cl]$_2$}$^{\bullet-}$ at E_1	2035sh/2023(s)	1915(s),br	
	2007(s)/1999sh		
{(μ-abpy)[Re(CO)$_3$Cl]$_2$}$^{\bullet-}$ at $E_{1'}$	2037(s)/2023sh	1945sh	
	2008sh/1986(s)	1913(s),br	
[(CO)$_3$Re(μ-abpy)Re(CO)$_3$Cl]$^-$ at E_2	2024(s)	1918sh	
	2002 (s)	1898(s),br	
		1885sh	
[(CO)$_3$Re(μ-abpy)Re(CO)$_3$Cl]$^-$ at $E_{2'}$	2023(s)		
	2017(s)	1905(s),br	
	1991(s)	1881(s)	

7. EPR spectroscopy

The radical complexes {(μ-abpy)[Re(CO)$_3$X]$_2$}$^{\bullet-}$ have been studied by X band EPR in this work (X = F, I) or earlier [7a,7b] (X = Cl, Br). Full EPR analysis was difficult because of the limited information. The dominant metal hyperfine splitting (from ^{185,187}Re, I = 5/2), the broadness of the lines due to quadrupolar effects, and unresolved halogen coupling from ^{19}F, ^{35,37}Cl, ^{79,81}Br or ^{129}I [10,27] not only obscure ^{1}H and ^{14}N hyperfine splittings from the presumably spin-bearing abpy ligand, they also preclude the analysis of the *g* factor anisotropy at X band frequency (9.5 GHz). Even though the *g* anisotropy is small for radicals with little metal

contribution to the Singly Occupied Molecular Orbital (SOMO), it should be enhanced by the large spin–orbit coupling constants ζ of heavy transition elements such as rhenium ($\zeta \approx 2000\ cm^{-1}$ [27]) or of the heavier halogens [10,31].

Contrary to the reported room temperature X band spectrum of $\{(\mu\text{-abpy})[Re(CO)_3Cl]_2\}^{\bullet-}$ [7a,7b] obtained through electrolysis of the neutral complex $\{(\mu\text{-abpy})[Re(CO)_3Cl]_2\}$, no resolution of the metal hyperfine splitting was detected for $\{(\mu\text{-abpy})[Re(CO)_3I]_2\}^{\bullet-}$. This is expected in analogy to the reported spectrum of $\{(\mu\text{-abpy})[Re(CO)_3Br]_2\}^{\bullet-}$ [7a,7b] and is attributed to the broadening of the signal due to unresolved halogen coupling.

The X-band EPR signal obtained from the stable radical complex $\{(\mu\text{-abpy})[Ru(CO)_3F]_2\}^{\bullet-}$ is also unrevealing. No $^{185,187}Re$ and ^{19}F splittings could be observed, in contrast to what was detected for the mononuclear complex [10]. The signal is very intense and rather narrow (peak-to-peak width: $\Delta H_{pp} = 3.1$ mT). This could be due to exchange-narrowing [27] caused by aggregation of the radicals. On electrolysis, a broader signal ($\Delta H_{pp} \approx 9$ mT) was obtained, uptake of another electron by the radical anion led to the formation of an EPR-silent species. The signal obtained after electrolysis looks more like the expected signal with hidden rhenium hyperfine splitting [7a,7b], however, the resolution was not good enough to obtain accurate values for the hyperfine coupling of $^{185,187}Re$ or ^{19}F. In any case, the g anisotropy observed at higher frequencies strongly suggests that the compound is a rhenium radical complex.

Since the g factor measurements had to be done for immobilized species, it was preferred to carry them out in frozen solutions at 5–40 K in order to minimize intermolecular dipolar interactions between the radicals. The samples consisted of saturated solutions of the starting complexes. Thus, the concentration was not the same for all studied samples, and when the complex had to be reduced *in situ* the available amount of radical species was not easily predictable.

The measurements at 230 and 285 GHz carried out at the Grenoble High Magnetic Field Laboratory gave satisfactory signal-to-noise ratios (Fig. 12).

In the following, the values obtained after electrolysis of the LT compound will be taken into account for the $\{(\mu\text{-abpy})[Re(CO)_3Cl]_2\}^{\bullet-}$ species, since this radical has been characterized earlier [7a,7b] in the X band by obtaining an eleven line pattern (corresponding to two rhenium centers interacting with one unpaired electron) at room temperature.

Measurements of the series $\{(\mu\text{-abpy})[Re(CO)_3X]_2\}^{\bullet-}$ (X = F, Cl, Br. I) at 285 GHz gave the spectra shown in Fig. 12. Experimental data as well as data obtained from DFT calculations [16] are summarized in Table 9.

The experimental g_{iso} values for $\{(\mu\text{-abpy})[Re(CO)_3X]_2\}^{\bullet-}$ are identical for the chloride and the bromide analogues (2.004). The values for the fluoride and iodide analogues are slightly greater (2.008). A relatively large g_{iso} value for the fluoride complex has already been observed for the mononuclear $[(abpy)Re(CO)_3F]^{\bullet-}$ [10], pointing to an orbital configuration where the SOMO lies closer to the HOMO than in the case of the chloride and bromide dinuclear complexes. Calculations reported earlier [16] overestimate g_{iso}.

The high-field measurements show a rhombic splitting with both negative and positive g shift (g–g_e) for all complexes $\{(\mu\text{-abpy})[Re(CO)_3X]_2\}^{\bullet-}$ (Fig. 12). The relatively small g anisotropy g_1–g_3 between 0.031 for the fluoride and 0.041 for the iodide derivative and the fact that the three g values are still rather close to $g_e = 2.0023$ are proof for the largely organic nature of the SOMO, involving H, C and N atoms but not Re or halides with large spin–orbit coupling constants. The anisotropy increases continuously but only slightly when going from fluoride to iodide. Calculations appear to satisfactorily reproduce the g anisotropy for the chloride and bromide derivatives. For the iodide species, the g anisotropy is overestimated, for $\{(\mu\text{-abpy})[Re(CO)_3F]_2\}^{\bullet-}$ the g anisotropy is slightly underestimated. The halide effect is clearly overestimated by DFT when comparing experimental and calculated g anisotropy values. Apparently there is only marginal spin transmission from the radical ligand via the rhenium metal atom to the halide co-ligands.

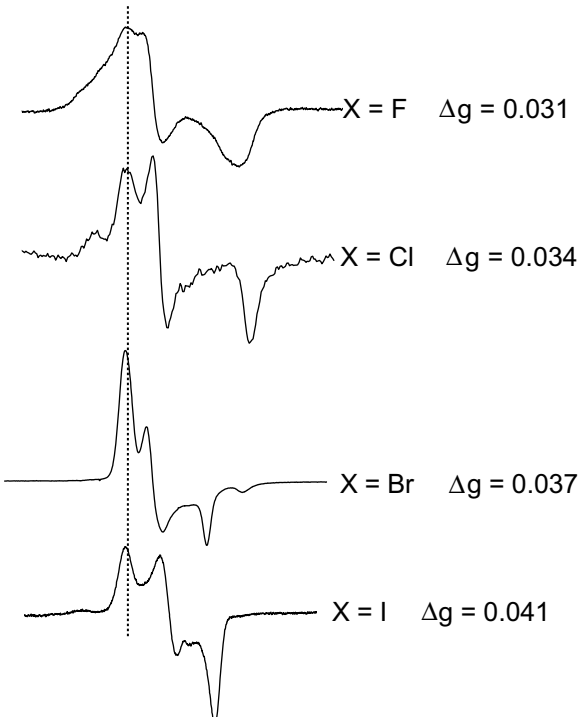

Fig. 12. High-field/high-frequency (285 GHz) EPR spectra of $\{(\mu\text{-abpy})[Re(CO)_3X]_2\}^{\bullet-}$ in CH_2Cl_2/toluene at 5 K showing the increase of the g anisotropy on going from X = F to I. Spectra were shifted to the same g_1 value to clearly see the change in anisotropy. For X = F, the isolated compound was measured as a stable radical, X = Cl, the radical was obtained through electrolysis, X = Br and I, the radicals were obtained through reduction with Zn.

Table 9
Experimental and computed[a] g values for the systems $\{(\mu\text{-abpy})[Re(CO)_3X]_2\}^{\bullet-}$

Complex		g_{iso}[b]	g_1[c]	g_2[c]	g_3[c]	Δg[d]
$\{(\mu\text{-abpy})[Re(CO)_3F]_2\}^{\bullet-}$	Exp.	2.008	2.014	2.007	1.983	0.031
	Calc.	2.005	2.014	2.006	1.995	0.019
$\{(\mu\text{-abpy})[Re(CO)_3Cl]_2\}^{\bullet-}$	Exp.	2.004[e]	2.019	2.009	1.984	0.034
	Calc.	2.012	2.029	2.013	1.995	0.035
$\{(\mu\text{-abpy})[Re(CO)_3Br]_2\}^{\bullet-}$	Exp.	2.004[e]	2.021	2.007	1.984	0.037
	Calc.	2.018	2.042	2.006	2.005	0.037
$\{(\mu\text{-abpy})[Re(CO)_3I]_2\}^{\bullet-}$	Exp.	2.008	2.030	2.010	1.989	0.041
	Calc.	2.041	2.084	2.042	1.995	0.088

[a] From DFT calculations, see Ref. [16].
[b] Experimental isotropic g value obtained from X band measurements in CH_2Cl_2 at 298 K.
[c] Experimental values obtained from measurements at 285 GHz in CH_2Cl_2/toluene at 5 K.
[d] $\Delta g = g_1 - g_3$.
[e] For hyperfine information see Refs. [7a,7b].

8. Conclusion

Our efforts to obtain and study the dinuclear complexes $\{(\mu\text{-abpy})[Re(CO)_3X]_2\}$ led to the isolation of structurally characterized neutral compounds, *anti*-$\{(\mu\text{-abpy})[Re(CO)_3X]_2\}$, X = Br ($I4_1/a$), I ($C2/c$). On the other hand, two crystalline forms of *anti*-$\{(\mu\text{-abpy})[Re(CO)_3Cl]_2\}$ were obtained, one of which ($P2_1/c$) had been reported before [9], while the other ($I4_1/a$), obtained through

crystallization in the presence of Zn, proved to be isostructural to the form found for *anti*-{(μ-abpy)[Re(CO)$_3$Br]$_2$}. Different synthetic procedures for {(μ-abpy)[Re(CO)$_3$Cl]$_2$} at high or low temperatures yielded different compositions, with the high temperature procedure leading to partial formation of *syn*/*anti* mixtures and to one-electron reduced species as evident from EPR. The same was observed to an even greater extent in the preparation of labile *syn*/*anti*-{(μ-abpy)[Re(CO)$_3$F]$_2$}$^{o/\bullet-}$. The identity of the isolated species as investigated by ^{1}H NMR spectroscopy, X-band and high-frequency EPR spectroscopy, cyclic voltammetry/polarography, UV/Vis- and IR-spectroelectrochemistry illustrated the effects of halide variation on the structural arrangement, on the reduction potentials decreasing from F to I, on the facilitated isomerization on going from I to F, and on the electronic situation in both the neutral and the radical anion complexes {(μ-abpy)[Re(CO)$_3$X]$_2$}$^{o/\bullet-}$. In a straightforward sense, the two new systems (μ-abpy)[Re(CO)$_3$X]$_2$ are distinguished by the large difference in electronegativity of X, the less electronegative X = I stabilizing the unreduced *anti* isomer while the most electronegative ligand X = F facilitates reduction (still centered on the abpy bridge) and electron-transfer induced [32] isomerization.

9. Experimental

9.1. 1. Instrumentation

EPR spectra in the X band were recorded with a Bruker System EMX. EPR spectra at 285 GHz were recorded using a multifrequency spectrometer [33]. A Gunn diode operating at 95 GHz and equipped with a third harmonic generator has been used as a radiation source. An InSb bolometer (QMC Instruments) was used for detection. The main magnetic field was provided by a superconducting magnet (Cryogenics Consultant) which generates fields up to 12 T. Owing to different field sweep conditions, the absolute values of the g components were obtained by calibrating the precisely measured g anisotropy data with the isotropic *g* value from X-band measurements. While this procedure does not account for the temperature dependence of g, the values extracted are identical with those obtained using an added standard. The accuracy of g values is estimated at ±0.0003. ^{1}H NMR spectra were taken on a Bruker AC 250 spectrometer. IR spectra were obtained using a Nicolet 6700 FT-IR instrument. UV–Vis–NIR absorption spectra were recorded on J&M TIDAS and Shimadzu UV 3101 PC spectrophotometers. Cyclic voltammetry was carried out in 0.1 M Bu_4NPF_6 solutions using a three-electrode configuration (glassy carbon working electrode, Pt counter electrode, Ag/AgCl reference) and a PAR 273 potentiostat and function generator. The ferrocene/ferrocenium (Fc/Fc^+) couple served as internal reference. Spectroelectrochemistry was performed using an optically transparent thin-layer electrode (OTTLE) cell [34a]. A two-electrode capillary served to generate intermediates for X band EPR studies [34b].

9.2. Syntheses

The preparation of {(μ-abpy)[Re(CO)$_3$Cl]$_2$} (LT and HT forms) and of {(μ-abpy)[Re(CO)$_3$Br]$_2$} has been reported previously [7a,7b,9].

9.2.1. {(μ-abpy)[Re(CO)$_3$F]$_2$}$^{o/\bullet-}$

Eighty milligrams (0.18 mmol) Re(CO)$_5$I and 140 mg (1.10 mmol) AgF were stirred in the dark for 2 h in 30 mL toluene. The AgI precipitate and the remaining AgF were filtered off (several times). A solution of 95 mg (0.20 mmol) (abpy)Re(CO)$_3$F in 5 mL toluene was added to the pale yellow solution. The mixture was stirred for 4 h at 55 °C. The green/brown solution was evaporated to half of its volume and 25 mL hexane was added. The solution was kept at −25 °C overnight. The green precipitate was filtered off and dried under vacuum. Due to a mixture of reduced form (90%, cation unknown) and non-reduced form (10%) as deduced from polarography, the isolated material could not be ascertained by elemental analysis. Spectroscopy (see main text) gave the following information:

{(μ-abpy)[Re(CO)$_3$F]$_2$}: IR (CH_2Cl_2): $\tilde{\nu}_{CO}$/cm^{-1} = 2056sh, 2020(vs), 2006sh, 1960sh, 1948(s), 1918(s). UV/Vis (CH_2Cl_2): λ_{max}/nm = 280sh, 340sh, 425, 700. ^{1}H NMR (CD_2Cl_2): δ = 9.30 (ddd, 2H, H^3), 9.23 (ddd, 2H, H^6), 8.31 (ddd, 2H, H^4), 7.82 (ddd, 2H, H^5).

{(μ-abpy)[Re(CO)$_3$F]$_2$}$^{\bullet-}$ (unknown counterion): IR (CH_2Cl_2): $\tilde{\nu}_{CO}$/cm^{-1} = 2019sh, 2009(s), 1921(s), 1903(s), 1892sh. UV/Vis (CH_2Cl_2): λ_{max}/nm = 275sh, 350, 380sh, 455, 480sh, 520sh, 620sh. EPR (CH_2Cl_2-toluene, 5 K): g_1 = 2.014, g_2 = 2.007, g_3 = 1.983.

9.2.2. {(μ-abpy)[Re(CO)$_3$I]$_2$}

One hundred and thirty milligrams (0.29 mmol) Re(CO)$_5$I and 25 mg (0.14 mmol) abpy were heated to reflux for 12 h in 40 mL of a 3:1 toluene–dichloromethane mixture. The deep green solution was evaporated to dryness. The solid was dissolved in a 40 mL 3:1 mixture of hexane–dichloromethane and cooled to −25 °C. After 5 h a deep green precipitate was collected, washed with hexane and dried under vacuum. Yield: 82 mg (0.07 mmol, 50%). Anal. Calc. for $C_{16}H_8I_2N_4O_6Re_2\times2\ CH_2Cl_2$ (1148.34 g/mol): C, 18.83; H, 1.05; N, 4.88. Found: C, 18.87; H, 0.93; N, 4.99%. IR (CH_2Cl_2): $\tilde{\nu}_{CO}$/cm^{-1} = 2042sh, 2012(vs), 1953(s), 1938(s). UV/Vis (CH_2Cl_2): λ_{max}/nm (ε/M^{-1} cm^{-1}) = 355(8200), 397(8200), 421(6600), 488(3600), 740sh, 826(5300). ^{1}H NMR (CD_2Cl_2): δ/ppm = 9.30 (ddd, 2H, H^3), 9.23 (ddd, 2H, H^6), 8.31 (ddd, 2H, H^4), 7.82 (ddd, 2H, H^5); $^3J_{3,4}$ = 8.6 Hz, $^3J_{4,5}$ = 7.5 Hz, $^3J_{5,6}$ = 5.5 Hz, $^4J_{3,5}$ = 1.2 Hz, $^4J_{4,6}$ = 1.6 Hz, $^4J_{3,6}$ = 0.7 Hz.

9.3. Crystallography

Single crystals of compounds (μ-abpy)[Re(CO)$_3$X]$_2$ were grown by layering dichloromethane solutions (X = Cl, Br) or an acetone solution (X = I) with slowly diffusing hexane. The two crystals which exhibited space group I4$_1$/a (X = Cl and Br), were obtained from solutions containing zinc powder.

Data collection was performed on the diffractometers NONIUS Kappa-CCD STOE IPDS. The structures were solved via direct methods using the programme SHELXS-97 [35]. Refinement was carried out by the full matrix least-squares method employing the programme SHELXL-97 [36]. All non-hydrogen atoms were refined anisotropically, hydrogen atoms were introduced at appropriate positions with coupled isotropic factors using the riding models. Absorption corrections were performed numerically using the programme HABITUS [37].

This work was supported by funding from the DFG (Graduate College "Magnetic Resonance"), the FCI, and the EU. We also acknowledge the fruitful cooperation with Prof. Dr. M. Kaupp and Dr. I. Ciofini.

Supplementary material

CCDC 699834, 699835, 699836 and 699837 contains the supplementary crystallographic data for this paper. These data can be obtained free of charge from The Cambridge Crystallographic Data Centre via www.ccdc.cam.ac.uk/data_request/cif.

References

[1] (a) D.P. Summers, J.C. Luong, M.S. Wrighton, J. Am. Chem. Soc. 103 (1981) 5238;
(b) W. Kaim, H.E.A. Kramer, C. Vogler, J. Rieker, J. Organomet. Chem. 367 (1989) 107.

[2] (a) A. Vlček Jr., M. Busby, Coord. Chem. Rev. 250 (2006) 1755;
(b) C. Shih, A.K. Museth, M. Abrahamsson, A.M. Blanco-Rodriguez, A.J. Di Bilio, J. Sudhamsu, B.R. Crane, K.L. Ronayne, M. Towrie, A. Vlček Jr., J.H. Richards, J.R. Winkler, H.B. Gray, Science 320 (2008) 1760;
(c) S.M. Contakes, G.A. Juda, D.B. Langley, N.W. Halpern-Manners, A.P. Duff, A.R. Dunn, H.B. Gray, D.M. Dooley, J.M. Guss, H.C. Freeman, PNAS 102 (2005) 13451;
(d) H. Hartmann, W. Kaim, I. Hartenbach, T. Schleid, M. Wanner, J. Fiedler, Angew. Chem. 113 (2001) 2927;
(e) H. Hartmann, W. Kaim, I. Hartenbach, T. Schleid, M. Wanner, J. Fiedler, Angew. Chem., Int. Ed. 40 (2001) 2842;
(f) H. Hartmann, W. Kaim, M. Wanner, A. Klein, S. Frantz, C. Duboc-Toia, J. Fiedler, S. Zalis, Inorg. Chem. 42 (2003) 7018;
(g) A.N. Maity, B. Sarkar, M. Niemeyer, M. Sieger, C. Duboc, S. Zalis, W. Kaim, Dalton Trans. (in press).
[3] J. Hawecker, J.M. Lehn, R. Ziessel, J. Chem. Soc., Chem. Commun. (1984) 328.
[4] B.P. Sullivan, T.J. Meyer, J. Chem. Soc, Chem. Commun. (1984) 1244.
[5] (a) J. Hawecker, J.M. Lehn, R. Ziessel, Helv. Chim. Acta 69 (1986) 1900;
(b) F.P.A. Johnson, M.W. George, F. Hartl, J.J. Turner, Organometallics 15 (1996) 3374;
(c) D.H. Gibson, H. He, Chem. Commun. (2001) 2082.
[6] T. Scheiring, A. Klein, W. Kaim, J. Chem. Soc., Perkin Trans. 2 (1997) 2569.
[7] (a) W. Kaim, S. Kohlmann, Chem. Phys. Lett. 139 (1987) 365;
(b) W. Kaim, S. Kohlmann, Inorg. Chem. 29 (1990) 2909;
(c) W. Matheis, W. Kaim, J. Chem. Soc., Faraday Trans. 86 (1990) 3337;
(d) B. Sarkar, S. Frantz, W. Kaim, C. Duboc, Dalton Trans. (2004) 3727.
[8] (a) A. Klein, C. Vogler, W. Kaim, Organometallics 15 (1996) 236;
(b) G.J. Stor, F. Hartl, J.W.M. Van Outersterp, D.J. Stufkens, Organometallics 14 (1995) 1115;
(c) B.D. Rossenaar, F. Hartl, D.J. Stufkens, Inorg. Chem. 35 (1996) 6194.
[9] H. Hartmann, T. Scheiring, J. Fiedler, W. Kaim, J. Organomet. Chem. 604 (2000) 267.
[10] S. Frantz, J. Fiedler, I. Hartenbach, Th. Schleid, W. Kaim, J. Organomet. Chem. 689 (2004) 3031.
[11] (a) P.S. Braterman, J.-I. Song, S. Kohlmann, C. Vogler, W. Kaim, J. Organomet. Chem. 411 (1991) 207;
(b) J. Fees, M. Ketterle, A. Klein, J. Fiedler, W. Kaim, J. Chem. Soc., Dalton Trans. (1999) 2595;
(c) S. Frantz, J. Rall, I. Hartenbach, T. Schleid, S. Zalis, W. Kaim, Chem. Eur. J. 10 (2004) 149.
[12] (a) S. Berger, A. Klein, W. Kaim, J. Fiedler, Inorg. Chem. 37 (1998) 5664;
(b) T. Scheiring, W. Kaim, J. Fiedler, J. Organomet. Chem. 598 (2000) 136;
(c) A. Klein, V. Kasack, R. Reinhardt, T. Sixt, T. Scheiring, S. Zalis, J. Fiedler, W. Kaim, J. Chem. Soc., Dalton Trans. (1999) 575.
[13] (a) K.D. Benkstein, J.T. Hupp, C.L. Stern, J. Am. Chem. Soc. 120 (1998) 12982;
(b) H. Hartmann, S. Berger, R. Winter, J. Fiedler, W. Kaim, Inorg. Chem. 39 (2000) 4977.
[14] (a) W. Kaim, N. Doslik, S. Frantz, T. Sixt, M. Wanner, F. Baumann, G. Denninger, H.-J. Kümmerer, C. Duboc-Toia, J. Fiedler, S. Zalis, J. Mol. Struct. 656 (2003) 183;
(b) S. Frantz, W. Kaim, J. Fiedler, C. Duboc, Inorg. Chim. Acta 357 (2004) 3657.
[15] B. Sarkar, W. Kaim, T. Schleid, I. Hartenbach, J. Fiedler, Z. Anorg. Allg. Chem. 629 (2003) 1353.
[16] S. Frantz, H. Hartmann, N. Doslik, M. Wanner, W. Kaim, H.-J. Kümmerer, G. Denninger, A.-L. Barra, C. Duboc-Toia, J. Fiedler, I. Ciofini, C. Urban, M. Kaupp, J. Am. Chem. Soc. 124 (2002) 10563.
[17] W. Kaim, Coord. Chem. Rev. 219-221 (2001) 463.
[18] W. Kaim, S. Kohlmann, J. Jordanov, D. Fenske, Z. Anorg. Allg. Chem. 598/599 (1991) 217.
[19] W. Kaim, S. Kohlmann, Inorg. Chem. 26 (1987) 68.
[20] (a) S. Kohlmann, S. Ernst, W. Kaim, Angew. Chem. 97 (1985) 698;
(b) S. Kohlmann, S. Ernst, W. Kaim, Angew. Chem., Int. Ed. Engl. 24 (1985) 684.
[21] M. Krejcik, S. Zalis, J. Klima, D. Sykora, W. Matheis, A. Klein, W. Kaim, Inorg. Chem. 32 (1993) 3362.
[22] M. Heilmann, S. Frantz, W. Kaim, J. Fiedler, C. Duboc, Inorg. Chim. Acta 359 (2006) 821.
[23] (a) T. Scheiring, J. Fiedler, W. Kaim, Organometallics 20 (2001) 1437. 3209;
(b) W. Kaim, T. Scheiring, M. Weber, J. Fiedler, Z. Anorg. Allg. Chem. 630 (2004) 1883;
(c) S. Berger, T. Scheiring, J. Fiedler, W. Kaim, Z. Anorg. Allg. Chem. 630 (2004) 2409;
(d) S. Frantz, M. Weber, T. Scheiring, J. Fiedler, C. Duboc, W. Kaim, Inorg. Chim. Acta 357 (2004) 2905;
(e) S. Frantz, R. Reinhardt, S. Greulich, M. Wanner, J. Fiedler, C. Duboc-Toia, W. Kaim, Dalton Trans. (2003) 3370.
[24] J.G. Dunn, D.A. Edwards, J. Organomet. Chem. 175 (1975) 199.
[25] A.-L. Barra, L.-C. Brunel, F. Baumann, M. Schwach, M. Moscherosch, W. Kaim, J. Chem. Soc., Dalton Trans. (1999) 3855.
[26] E. Horn, M.R. Snow, Aust. J. Chem. 34 (1981) 737.
[27] J.A. Weil, J.R. Bolton, Electron Paramagnetic Resonance, 2nd ed., Wiley, Hobokon, NJ, 2007.
[28] B. Sarkar, S. Patra, J. Fiedler, R.B. Sunoj, D. Janardanan, G.K. Lahiri, W. Kaim, J. Am. Chem. Soc. 130 (2008) 3532.
[29] (a) N. Doslik, T. Sixt, W. Kaim, Angew. Chem. 110 (1998) 2521;
(b) N. Doslik, T. Sixt, W. Kaim, Angew. Chem., Int. Ed. Engl. 37 (1998) 2403.
[30] N.G. Connelly, W.E. Geiger, Chem. Rev. 96 (1996) 877.
[31] V. Lorenzen, W. Preetz, F. Baumann, W. Kaim, Inorg. Chem. 37 (1998) 4011.
[32] (a) A.J.L. Pombeiro, in: A.J.L. Pombeiro, C. Amatore (Eds.), M.F.C. Guedes da Silva in Trends in Molecular Electrochemistry, Marcel Dekker, New York, 2004;
(b) W. Bruns, W. Kaim, M. Ladwig, B. Olbrich-Deussner, T. Roth, B. Schwederski, in: A.J.L. Pombeiro, J. McCleverty (Eds.), Molecular Electrochemistry of Inorganic, Bioinorganic and Organometallic Compounds, Kluwer Academic Publishers, Dordrecht, 1993, p. 255 (Nato ASI Series C 385).
[33] A.-L. Barra, L.-C. Brunel, J.-B. Robert, Chem. Phys. Lett. 165 (1990) 107.
[34] (a) M. Krejcik, M. Danek, F. Hartl, J. Electroanal. Chem. 317 (1991) 179;
(b) W. Kaim, S. Ernst, V. Kasack, J. Am. Chem. Soc. 112 (1990) 173.
[35] G.M. Sheldrick, Programme SHELXS, Göttingen, 1997.
[36] G.M. Sheldrick, Programme SHELXL, Göttingen, 1997.
[37] W. Herrendorf, H. Bärnighausen, Programme HABITUS, Gießen, Karlsruhe, 1993, Gießen, 1996.
[38] H. Bock, R. Dienelt, H. Schödel, T.T.H. Van, Struct. Chem. 98 (1998) 279.